Proton transport and torque generation in rotary biomotors

A. Yu. Smirnov,[1] S. Savel'ev,[1,2] L. G. Mourokh,[1,3] and Franco Nori[1,4]
[1]*Advanced Science Institute, The Institute of Physical and Chemical Research (RIKEN), Wako-shi, Saitama, 351-0198, Japan*
[2]*Department of Physics, Loughborough University, Loughborough LE11 3TU, United Kingdom*
[3]*Department of Physics, Queens College, The City University of New York, Flushing, New York 11367, USA*
[4]*Center for Theoretical Physics, Physics Department, The University of Michigan, Ann Arbor, Michigan 48109-1040, USA*
(Received 19 December 2007; revised manuscript received 29 May 2008; published 24 September 2008)

We analyze the dynamics of rotary biomotors within a simple nanoelectromechanical model, consisting of a stator part and a ring-shaped rotor having 12 proton-binding sites. This model is closely related to the membrane-embedded F_0 motor of adenosine triphosphate (ATP) synthase, which converts the energy of the transmembrane electrochemical gradient of protons into mechanical motion of the rotor. It is shown that the Coulomb coupling between the negative charge of the empty rotor site and the positive stator charge, located near the periplasmic proton-conducting channel (proton source), plays a dominant role in the torque-generating process. When approaching the source outlet, the rotor site has a proton energy level higher than the energy level of the site, located near the cytoplasmic channel (proton drain). In the first stage of this torque-generating process, the energy of the electrochemical potential is converted into potential energy of the proton-binding sites on the rotor. Afterwards, the tangential component of the Coulomb force produces a mechanical torque. We demonstrate that, at low temperatures, the loaded motor works in the shuttling regime where the energy of the electrochemical potential is consumed without producing any unidirectional rotation. The motor switches to the torque-generating regime at high temperatures, when the Brownian ratchet mechanism turns on. In the presence of a significant external torque, created by ATP hydrolysis, the system operates as a proton pump, which translocates protons against the transmembrane potential gradient. Here we focus on the F_0 motor, even though our analysis is applicable to the bacterial flagellar motor.

DOI: 10.1103/PhysRevE.78.031921 PACS number(s): 87.16.Nn, 85.85.+j

I. INTRODUCTION

Biological rotary motors, such as the F_0 motor of adenosine triphosphate (ATP) synthase and the bacterial flagellar motor (BFM), convert energy of the transmembrane electrochemical potential into mechanical motion [1,2]. The gradient of the electrochemical potential in the living cells is maintained by the metabolic mechanism that translocates ions (here protons) from the negative (or cytoplasmic) side of the membrane to its positive (periplasmic) side [1,3–5]. A mechanical torque is generated when protons flow down the electrochemical gradient across the mitochondrial or cell membranes [6–15]. Bacteria employs this torque directly for chemotaxis [16], whereas in ATP synthase the rotational energy is transmitted to the F_1 motor mechanically linked to the F_0 portion. The out-of-membrane component F_1 contains three sites, which harness the energy of mechanical rotations to catalyze the synthesis of ATP molecules. In the following, we concentrate on the F_0 motor, although our theoretical analysis can be applied to the BFM as well, since these motors have many common features.

A. Structure of the biomotor

The F_0 motor is embedded into a plasma membrane of bacteria or into an inner mitochondrial membrane. It consists of two components: (i) A stator or subunit *a*, tightly attached to the membrane, and (ii) a cylinder-shaped rotor (subunit *c*), which can freely rotate around its axis (Fig. 1). In the majority of models [7–13] the rotor contains several (10 to 15) proton-binding sites located in the middle of the membrane. The stator has two noncollinear half-channels, which are perpendicular to the plane of Fig. 1. Each one of these channels are connected either to the periplasmic side of the membrane, having a higher electrochemical potential, or to the cytoplasm, characterized by a lower potential. The source (*S*) half-channel delivers protons from the periplasm (the positive, or, *P* side of the membrane) to the rotor-stator interface, and, finally, to the proton-binding sites in the rotor plane. The drain (*D*) channel translocates protons from this interface to the cytoplasmic, or negative, *N* side of the membrane. The rotor sites can be protonated or deprotonated when they are in the immediate vicinity of the source or drain channels. In ATP synthase from *Escherichia coli* the residues *c*Asp-61 are equally placed along the rotating ring and serve as proton-binding sites carrying protons from the source to the drain channel [11]. An empty rotor site has a negative charge.

B. Motor mechanisms: Brownian ratchet and power stroke

It is assumed [7,8] that protons, delivered to the left-hand side (Fig. 1) of the rotor-stator interface by the source channel, bind and neutralize the empty rotor sites, and after that, travel clockwise [looking from the upper, periplasmic, side of the membrane, as shown in Fig. 1(a)]. Notice that all rotor sites outside of the rotor-stator interface are occupied with protons and have no electric charge. The unprotonated negatively charged sites cannot face the lipid core of the membrane because of a large ($\geqslant$500 meV) desolvation penalty [17]. The proton escapes from the rotor during the process of clockwise-directed rotor diffusion, when the corresponding site approaches the drain (cytoplasmic) channel located at the

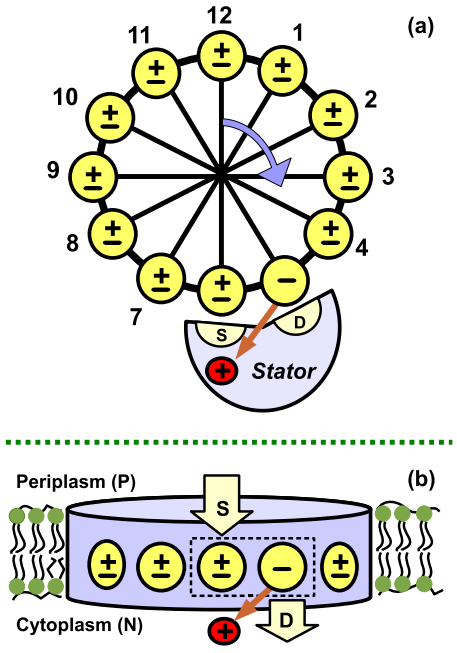

FIG. 1. (Color online) Schematic diagram of a rotary nanomotor powered by an electrochemical potential gradient. (a) shows the top view from the periplasmic (*P*) side of the membrane; (b) shows the side view. Panel (a) shows the rotor, which has 12 sites which rotate as a Ferris wheel. In the example shown in (a), the site number "5" provides a proton to the drain (*D*) channel of the stator, and the proton then moves to the cytoplasm, as shown in (b). This now negatively charged site number "5" in (a) feels a Coulomb attraction from the positive (red) stator charge, which propels the wheel to rotate an angle $\phi_0=30°$. After site number "5" moves to the location of the next site, the source (*S*) donates a proton to that site, neutralizing it, and the 30° rotation process is ready to start all over again. In (b), the protons, indicated by "+," move from the periplasm (*P*), which acts as a source (*S*), to the cytoplasm (*N*), acting as a proton drain (*D*), on the other side of the membrane. In (a) and (b), an orange straight arrow represents the Coulomb force between the empty rotor site and the positive stator charge.

right-hand side of the rotor-stator strip (Fig. 1). The negatively charged empty site is not able to move back now because of the strong repulsion of the lipid medium. However, it can diffuse forward, in the clockwise (CW) direction, since there is no energy penalty for the charge placed inside the hydrophilic rotor-stator interface. The site is populated and neutralized again when it reaches the source channel at the left-hand side of the interface, and the wheel can continue its CW rotation.

Because of random thermal forces, the rotor can also rotate in the counterclockwise (CCW) direction, and the populated site would then approach the drain channel. In the most probable event, the site is depopulated and reflected from the lipid border of the rotor-stator interface. However, with a smaller probability, the neutral site, occupied with a proton, crosses the border, and the wheel rotates counterclockwise. When the population of the rotor sites occurs on the left-hand side of the rotor-stator interface, and the depopulation happens on the right-hand side, the rotor diffusion is biased to rotate CW. This means that the F_0 motor works as a Brownian ratchet [18–20].

References [8,10,21] have shown, however, that the Brownian ratchet model is not able to explain the operation of the F_0 motor in the presence of an external torque (about 41 pN nm), which is produced by the F_1 motor and acts in the opposite (CCW) direction. In addition to two half-channels, the stator contains a positive charge (a residue *a*Arg-210 in *E. coli*) which can be located between two proton-conducting half-channels in the rotor plane [8,11]. As schematically shown in Fig. 1(a), upon passing the source channel, the rotor site releases its proton and becomes negatively charged. This charge is attracted by the positive residue, thereby generating a torque moving the rotor in the CW direction (power stroke component). Reference [8] has demonstrated that the positive stator charge is necessary for the efficient reverse operation of ATP synthase, when it works as a proton pump under the action of the external torque produced by ATP hydrolysis. The irreplaceable role of the *a*Arg-210 residue for the ATP-driven pumping activity of the F_0F_1 complex in *E. coli* has been proven by direct mutagenesis studies [22]. It should be noted that, despite the recent significant progress in understanding the operation of ATP synthase, the physical mechanism of the torque generation and proton translocation by the F_0 motor calls for further investigation [12,13]. Of special interest is the possibility to mimic the main features of this biological engine with the goal to create an artificial nanomachine with an almost perfect energy conversion.

C. Quantitative modeling

Here we explore a simple model incorporating the most important aspects of biomolecular rotary motors [7–11] and employing a quantitative treatment based on methods of condensed matter physics [5,23,24]. These approaches have been previously applied to nanoelectromechanical systems (NEMS) with their mechanical motion affecting the electrical properties of electronic devices [25]. Similar processes take place in nanoscale biological objects, where electrical and mechanical degrees of freedom are also strongly coupled, making them living counterparts to artificial NEMS. Note that only nanooscillators have been extensively studied by theorists, although a single-molecule rotor and nanoelectromechanical rotational actuators [26] have been demonstrated experimentally. To the best of our knowledge, no theoretical investigations of rotary NEMS have been reported yet. It can be expected that artificial nanoengines built on the operating principles of biological motors could achieve the same level of efficiency and performance.

ATP synthase, along with many other enzymes [4], should be considered as a nonequilibrium open system whose operation is supported by a permanent flow of protons. To describe this flow we attach the F_0 motor to two proton reservoirs related to the periplasmic (positive, *P*) side of the membrane and to the cytoplasmic (negative, *N*) side of the membrane. In the case of the respiratory chain [1], the *P* side and the *N* side correspond to the intermembrane space and to the matrix, respectively, divided by an inner mitochondrial membrane. Usually the proton transfer between the rotor sites and the *P* and *N* aqueous sides of the membrane is

represented by a set of Markov equations with a phenomenologically constructed transition matrix [9,15,21]. Here, with the methods of quantum transport theory [5,23–25], we derive the rate equations and provide simple expressions for transition coefficients, which explicitly depend on the difference between electrochemical potentials of the proton reservoirs and on the distance between the proton-binding sites on the rotor and on the stator. This approach gives a clear physical picture of the loading and unloading events as well as the torque-generation process as a whole.

The paper is organized as follows. In Sec. II we describe in detail the model and formulate the Hamiltonian of the system. In Sec. III we present a Langevin equation for the mechanical motion of the rotor and derive the rate equations for the populations of the proton-binding sites on the rotor. In Sec. IV we numerically solve the equations of motion and discuss our results. Section V is devoted to conclusions.

II. MODEL

We consider 12 equally spaced proton-binding sites ($\sigma=1,\ldots,12$), attached to a ring-shaped rotor (c-subunit) of radius r_0, at the points with the angular coordinates $\phi_\sigma=\sigma\phi_0$, where $\phi_0=\pi/6$ is the angular distance between the rotor sites. Then, if the rotor is turned through an angle ϕ, the proton-binding site σ has a coordinate

$$\mathbf{r}_\sigma=\{r_0\sin(\phi+\phi_\sigma),\quad r_0\cos(\phi+\phi_\sigma)\}.$$

We choose the coordinate origin at the center of the rotor wheel. As shown in Fig. 1, the stator part of the motor (or a subunit) contains the source half-channel, S, which delivers protons from the P side (periplasm) of the membrane to the point with an angular position $\phi_S=\pi$ on the rotor-stator interface. The drain half-channel, D, also belonging to the stator, connects the point $\phi_D=\pi-\phi_0$ with the cytoplasmic (N) side of the membrane. Also, the stator has a positive charge $q|e|$ located in the rotor plane on the y axis, with coordinates $\mathbf{r}_q=\{0,-r_0-d\}$. Here d is the distance from the charge $q|e|$ to the closest proton-binding site on the rotor, e is the electron charge. As a result, the Hamiltonian of the system has the form

$$H=H_\phi+\sum_{k\alpha}E_{k\alpha}c_{k\alpha}^+c_{k\alpha}+H_{\rm tun}+\sum_\sigma E_\sigma n_\sigma+\sum_\sigma[U_q(\phi+\phi_\sigma)+U_{\rm con}(\phi+\phi_\sigma)](1-n_\sigma),\tag{1}$$

where the Hamiltonian H_ϕ governs the mechanical motion of the cylinder-shaped rotator, characterized by the angle ϕ, counted clockwise from the y axis. The occupation of the proton-binding site σ, having eigenenergy E_σ, is described by the creation and annihilation operators of protons, a_σ^+, a_σ, with a corresponding population operator $n_\sigma=a_\sigma^+a_\sigma$. Fermi operators $c_{k\alpha}^+$, $c_{k\alpha}$ are related to the state, with momentum k, of the proton in the source and drain reservoirs ($\alpha=S,D$) with energy $E_{k\alpha}$. The Hamiltonian $H_{\rm tun}$ describes the proton transfer between the proton-binding sites on the rotor and the source and drain channels on the stator.

A. Coulomb interactions

The empty site (with $n_\sigma=0$) has a negative charge, and, because of this, it is attracted by the stator charge $q|e|$. The screened Coulomb coupling between the negative charge, $-|e|$, of the empty rotor site and the positive stator charge $q|e|$, separated by the angular-dependent distance $r_q(\phi+\phi_\sigma)=|\mathbf{r}_\sigma-\mathbf{r}_q|$, is determined by the potential [11]

$$U_q(\phi+\phi_\sigma)=-\frac{qe^2}{4\pi\varepsilon_0\varepsilon r_q(\phi+\phi_\sigma)}\exp\left(-\frac{r_q(\phi+\phi_\sigma)}{r_s}\right),\tag{2}$$

where ε_0 is the electric permittivity, ε is the dielectric constant of the medium, r_s is the Debye screening length, and

$$r_q(\phi+\phi_\sigma)=\sqrt{r_0^2+(r_0+d)^2+2r_0(r_0+d)\cos(\phi+\phi_\sigma)}.\tag{3}$$

To take into account an energetic penalty for the charged rotor site σ, when it faces a lipid bilayer outside of the rotor-stator strip, we introduce a confinement potential,

$$U_{\rm con}(\phi+\phi_\sigma)=U_c\{1-\exp[-\lambda_c[1-\cos(\phi+\phi_\sigma-\phi_c)]^2]\},\tag{4}$$

where an angle ϕ_c corresponds to the middle of the rotor-stator strip, $\phi_c=\pi-\phi_0/2$, a parameter λ_c is inversely proportional to the width of the interface, and a potential U_c represents a desolvation penalty. The transfer of an ion with charge $-|e|$ from water (with a dielectric constant ε_1) to the hydrophobic membrane (having a constant ε_2) is subject to the energy penalty [17],

$$U_c({\rm meV})=\frac{1440e^2}{2a}\left(\frac{1}{\varepsilon_2}-\frac{1}{\varepsilon_1}\right),\tag{5}$$

where a is the size of the cavity (in nm) over which the charge is spread. For $\varepsilon_1=80$, $\varepsilon_2=3$, and $a=0.2$ nm, the desolvation energy is about $U_c=1160$ meV. We assume here that the proton-proton Coulomb interaction between sites is small enough, so that the loading and unloading of different sites occurs independently.

B. Proton transfer

Protons in the source and drain reservoirs are characterized by the Fermi distributions,

$$f_\alpha(\omega)=\left[\exp\left(\frac{\omega-\mu_\alpha}{T}\right)+1\right]^{-1},\tag{6}$$

with temperature T ($\hbar=1$, $k_B=1$) and electrochemical potentials $\mu_S=V/2$, $\mu_D=-V/2$, where V is the proton voltage build-up, in units of energy, meV. For ATP synthase in *Escherichia coli*, protons can be translocated from the aqueous sides of the membrane to the rotor-stator interface by a set of hydrogen-bonded chains [27]. The mechanism of a proton transfer between the rotor sites cAsp-61 and the terminal residues of the source channel, aAsn-214, and the drain channel, aSer-206, is not completely understood. However, molecular dynamics simulations [11] demonstrate that hy-

drogen bonds can be formed between the proton-binding sites on the rotor (*c*Asp-61) and the terminal residues (*a*Asn-214 or *a*Ser-206). These bonds are able to transfer protons within picoseconds either by collective tunneling [27], or, which is more probable, by classical hopping [8,11]. The proton translocation process strongly depends on the distance between the rotor sites and the stator residues and, at the molecular level, it can be facilitated by internal rotations of transmembrane helices as well as by the motion of other key elements [11,28,29]. In our simplified model, we mimic the stator-rotor proton transitions with the Hamiltonian

$$H_{\rm tun} = -\sum_{k\alpha\sigma} (T_{k\alpha} c_{k\alpha}^{+} a_{\sigma} + T_{k\alpha}^{*} a_{\sigma}^{+} c_{k\alpha}) w_{\alpha}(\phi + \phi_{\sigma}), \qquad (7)$$

which describes the effective proton tunneling with amplitudes $T_{k\alpha}$, multiplied by factors $w_{\alpha}(\phi+\phi_{\sigma})$. The factors $w_{\alpha}(\phi+\phi_{\sigma})$ depend on the distance between the site σ and the final residue of the α-channel located at the point $\mathbf{r}_{\alpha} = \{r_0 \sin \phi_{\alpha}, r_0 \cos \phi_{\alpha}\}$,

$$|\mathbf{r}_{\sigma} - \mathbf{r}_{\alpha}| = \sqrt{2} r_0 \sqrt{1 - \cos(\phi + \phi_{\sigma} - \phi_{\alpha})}. \qquad (8)$$

We approximate this dependence by the exponential function,

$$w_{\alpha}(\phi + \phi_{\sigma}) = \exp(-\lambda_r |\mathbf{r}_{\sigma} - \mathbf{r}_{\alpha}|), \qquad (9)$$

characterized by a steepness λ_r. The value of λ_r is inversely proportional to the size of the molecular groups participating in the proton transport (either *c*Asp-61 and *a*Asn-214, or *a*Ser-206). It should be noted that the specific functional form of the factor $w_{\alpha\sigma}(\phi)$ is not crucial for the model under study.

III. EQUATIONS OF MOTION

The viscous medium creates a torque,

$$\mathcal{T}_r = \zeta_r \frac{d\phi}{dt}, \qquad (10)$$

acting on the cylinder-shaped rotor, together with a stochastic force ξ. For a cylinder with radius r_0 and height h, rotating in a medium with viscosity η, the drag coefficient ζ_r is defined by the formula [30,31]:

$$\zeta_r = 4\pi\eta r_0^2 h. \qquad (11)$$

It follows from the Hamiltonian (1), that the processes of loading and unloading of protons at the rotor-stator interface generates an additional torque. Thus, the following Langevin equation describes the biased overdamped diffusion of the rotor:

$$\zeta_r \dot{\phi} = \xi + \mathcal{T}_{\rm ext} - \sum_{\sigma} (1 - n_{\sigma}) \frac{d}{d\phi} [U_q(\phi + \phi_{\sigma}) + U_{\rm con}(\phi + \phi_{\sigma})]. \qquad (12)$$

Here $\xi(t)$ is a zero-mean value Gaussian fluctuation source, characterized by the correlation function: $\langle \xi(t)\xi(t')\rangle = 2T\zeta_r \delta(t-t')$, and $\mathcal{T}_{\rm ext}$ is an external torque produced by the F_1 motor. We expect that the F_0 motor will rotate in the CW direction (looking from the periplasm side of the membrane). Therefore, the torque from F_1, which decelerates this motion, should have a negative sign, $\mathcal{T}_{\rm ext} < 0$. The effects of the rotor-stator proton transitions on the mechanical motion, resulting from the Hamiltonian $H_{\rm tun}$, are assumed to be negligibly small.

The "chemical" part of the problem, namely, the process of loading and unloading the proton-binding sites on the rotor, is governed by the Heisenberg equations for the population operators, $n_{\sigma} = a_{\sigma}^{+} a_{\sigma}$, which can be derived [5,24] from Eqs. (1) and (7),

$$\dot{n}_{\sigma} = i \sum_{k\alpha} (T_{k\alpha}^{*} a_{\sigma}^{+} c_{k\alpha} - T_{k\alpha} c_{k\alpha}^{+} a_{\sigma}) w_{\alpha}(\phi + \phi_{\sigma}), \qquad (13)$$

where the reservoir operators, $c_{k\alpha}$, are represented as a sum of the free term, $c_{k\alpha}^{(0)}$, and the term describing the reservoir response

$$c_{k\alpha} = c_{k\alpha}^{(0)} - T_{k\alpha} \sum_{\sigma} \int dt_1 g_{k\alpha}^{r}(t,t_1) a_{\sigma}(t_1) w_{\alpha\sigma}(t_1). \qquad (14)$$

Here

$$g_{k\alpha}^{r}(t,t_1) = -i \exp[-iE_{k\alpha}(t-t_1)]\theta(t-t_1)$$

is the retarded Green function of the α-reservoir, $\theta(t-t_1)$ is the Heaviside step function, and

$$w_{\alpha\sigma}(t) \equiv w_{\alpha}(\phi(t) + \phi_{\sigma}).$$

The correlator of the free reservoir operators is determined by the Fermi-distribution function $f_{\alpha}(E_{k\alpha})$,

$$\langle c_{k\alpha}^{(0)+}(t) c_{k\alpha}^{(0)}(t_1)\rangle = f_{\alpha}(E_{k\alpha}) \exp[iE_{k\alpha}(t-t_1)].$$

On substituting Eq. (14) into Eq. (13), and averaging the latter equation over the fluctuations of the proton reservoirs, we obtain

$$\langle \dot{n}_{\sigma}\rangle + \sum \Gamma_{\alpha} w_{\alpha\sigma}^2(t) \langle n_{\sigma}\rangle = \sum_{\alpha} |T_{k\alpha}|^2 \int dt_1 f_{\alpha}(E_{k\alpha}) e^{iE_{k\alpha}(t-t_1)} w_{\alpha\sigma}(t) w_{\alpha\sigma}(t_1) \times \langle [a_{\sigma}(t), a_{\sigma}^{+}(t_1)]_{+}\rangle \theta(t-t_1) + \text{H.c.} \qquad (15)$$

We introduce here the transition rates between the proton-binding sites and the reservoirs,

$$\Gamma_{\alpha} = 2\pi \sum_{k} |T_{k\alpha}|^2 \delta(E - E_{k\alpha}),$$

which are independent of energy in the wide-band limit approximation. Assuming weak coupling between the sites and the reservoirs, we employ free-evolving proton operators, $a_{\sigma}(t) = e^{-i\bar{E}_{\sigma}(t-t_1)} a_{\sigma}(t_1)$, to calculate the anticommutator in Eq. (15). Here

$$\bar{E}_{\sigma} = E_{\sigma} - U_q(\phi + \phi_{\sigma}) - U_{\rm con}(\phi + \phi_{\sigma}), \qquad (16)$$

is the total eigenenergy of the proton on the site σ including contributions of the stator charge potential, $U_q(\phi)$, and the confining potential, $U_{\rm con}(\phi)$. As a result, we derive a set of

rate equations for the populations n_σ, partially averaged over the Fermi distributions of the proton reservoirs,

$$\dot{n}_\sigma + \sum_\alpha \Gamma_{\alpha\sigma}(\phi) n_\sigma = \sum_\alpha \Gamma_{\alpha\sigma}(\phi) f_\alpha(\bar{E}_\sigma). \tag{17}$$

Hereafter we drop the averaging brackets $\langle \cdots \rangle$ and introduce the angular-dependent transition coefficients,

$$\Gamma_{\alpha\sigma}(\phi) = \Gamma_\alpha w_\alpha^2[\phi(t) + \phi_\sigma].$$

The rate equations (17) replace the phenomenological Markovian equations [9,15,21], which are usually employed for a description of the loading and unloading of the rotor sites. The characteristic time of proton transfer to and out of the proton-binding sites [8,11] is much shorter than the time scale of the rotation angle ϕ. Accordingly, we can average the stochastic equation (12) over fluctuations of the proton reservoirs without averaging over the fluctuations of the mechanical heat bath. The partially averaged proton population n_σ, involved in Eq. (12), depends on the local fluctuating value of the rotor angle $\phi(t)$. In the next section we solve numerically the stochastic equation (12) together with the system of rate equations (17) and investigate various regimes of the rotary nanomotor.

IV. RESULTS

We consider a cylinder-shaped motor with radius $r_0 = 3$ nm and height $h = 6$ nm, rotating in a medium with viscosity coefficient $\eta = 1$ Pa s, which is 1000 times higher than the viscosity of water. For a protein environment, surrounding the stator charge $q|e|$ and having a dielectric constant $\varepsilon = 3$, the energy of the Coulomb coupling $U_q(\phi)$ (2) is proportional to the factor $qe^2/(4\pi\varepsilon_0\varepsilon) = q \times 480$ meV nm. The Debye screening radius is $r_s = 1$ nm. We also assume that both, the stator charge and the end of the source channel, are located in the rotor plane on the y axis with $\phi_S = \pi$, and that the stator charge is offset by the minimum distance $d = 0.9$ nm from the circumference of the rotor ring. The drain channel is shifted to the right-hand side by the angle ϕ_0, $\phi_D = \pi - \phi_0$. For the steepness λ_r involved in the function $w_\alpha(\phi)$, we choose the value $\lambda_r = (0.25\ \text{nm})^{-1}$. The confinement potential (4) is characterized by the parameters $U_c = 1160$ meV, $\lambda_c = 20$. We assume that all proton-binding sites ($\sigma = 1, \ldots, 12$) have the same eigenenergy, $E_\sigma = E_0$. The proton transport through the system occurs if the ϕ-dependent energy levels of the proton-binding sites, $E(\phi) = E_0 - U_q(\phi) - U_{\text{con}}(\phi)$, located near the source and drain half-channels, $\phi = \phi_S$, ϕ_D, fit the transport window

$$\frac{V}{2} > E(\phi_S) > E(\phi_D) > -\frac{V}{2}. \tag{18}$$

The energy $E_0 = -90$ meV gives the values $E(\phi_D) = -84$ meV, $E(\phi_S) = 100$ meV, which meet these conditions at the transmembrane potential $V = 250$ meV. It is assumed that the time scales for transitions of protons between the reservoirs and the rotor sites are about $\Gamma_S^{-1} = \Gamma_D^{-1} = 0.5$ μs.

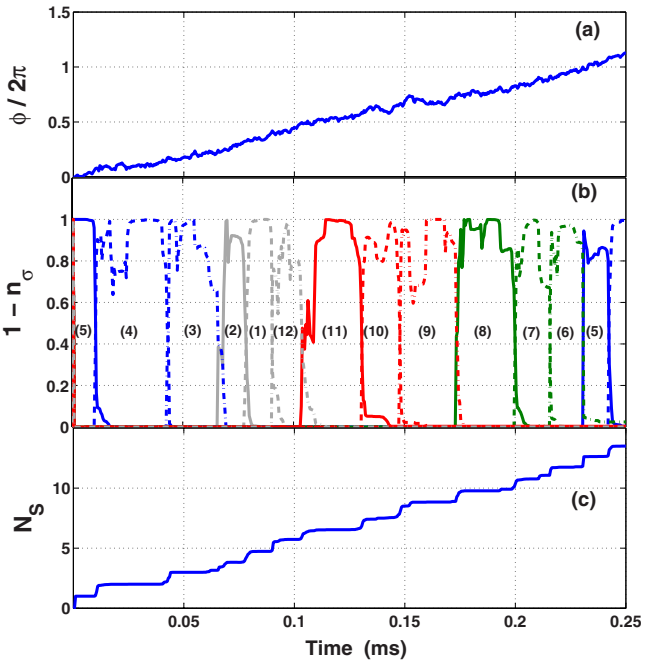

FIG. 2. (Color online) (a) Time dependence of the number of full rotations $\phi(t)/2\pi$ at $V = 250$ meV, $\mathcal{T}_{\text{ext}} = -41$ pN nm, $E_0 = -90$ meV, and at $T = 300$ K; (b) depopulations of the proton-binding sites, $\bar{n}_\sigma = (1 - n_\sigma)$, $\sigma = 1, \ldots, 12$, versus time (in ms); (c) the number of protons, N_S, transferred from the source to the drain reservoir, versus time (in ms). Notice the periodicity in (b). It follows from (a), that the motor performs a bit more than one full CW rotation for a period of time ~ 0.25 ms. This rotation is accompanied by the cyclic loading and unloading of the proton-binding sites on the rotor (b), starting with the site number "5" [see Fig. 1(a) and part (b) of this figure]. All sites were populated at the initial time $t = 0$. The rotor works as a Ferris wheel carrying protons from the source reservoir S to the drain D. The number of protons, N_S, translocated from the source to the drain, increases stepwise during the rotation of the wheel (c). Almost 12 protons are transferred through the 12-site system after the full circle, as seen in (c).

A. Rotations and site depopulations

In Fig. 2(a) we plot a number of full rotations, $\phi(t)/2\pi$, as a function of time (in ms), obtained from the numerical solution of the Langevin equation (12), coupled to the rate equations (17), at the source-drain voltage $V = 250$ meV, the stator charge $|e|$ ($q = 1$), and at temperature $T = 300$ K. We take into account here the constant load torque from the F_1 motor, $\mathcal{T}_{\text{ext}} = -41$ pN nm, which is enough to produce three ATP molecules per rotation of the F_1 motor.

In the initial state all sites are occupied with protons, and, because of this, are electrically neutral. The process of site depopulation is illustrated in Fig. 2(b), where we plot the probability to have the empty σ site, $\bar{n}_\sigma = 1 - n_\sigma$, as a function of time for $\sigma = 1, \ldots, 12$. The maximum value of $\bar{n}_\sigma$ on this graph corresponds to the unoccupied proton-binding site σ. The site "5" is depopulated in the first turn, because it is initially in the closest position to the drain channel. The empty site is attracted by the positive stator charge, and this force turns the rotor by an angle $\pi/6$ [see Fig. 2(a)]. The site "5" is occupied again when it reaches the source channel. In

Fig. 2(c) we plot the number N_S of protons, transferred from the source reservoir, as a function of time. It is evident from Fig. 2(c) that loading the site "5" is accompanied by the transfer of a proton from the source channel. The depopulation of the site "4" begins at the same time as the depopulation of the site "5." This process repeats over and over, resulting in a continuous unidirectional rotation of the rotary ring. The loaded motor makes a complete turn in a time interval ~0.25 ms, which corresponds to the frequency of rotations near 4 kHz; in so doing the system translocates about 12 protons down the potential gradient of 250 meV.

It should be noted that here we have an asymmetric configuration, where the energy level of the proton near the source channel is higher than the proton energy near the drain outlet, $E(\phi_S) > E(\phi_D)$. The energy drop,

$$\Delta E = E(\phi_S) - E(\phi_D) = U_q(\phi_D) - U_q(\phi_S), \qquad (19)$$

is directly converted into mechanical energy by the F_0 motor. We note that $U_q(\phi) < 0$ and $U_{\rm con}(\phi_S) = U_{\rm con}(\phi_D)$. At the opposite sign of the transmembrane potential difference, $V < 0$, the motor does not produce any unidirectional rotation, since in this case the proton energies do not fit the transport window (18).

B. Torque generation and shuttling

In Fig. 3 the average rotational frequency, $\langle\Omega\rangle/2\pi = \langle\dot{\phi}\rangle/2\pi$, shown in (a), and the proton current, $I_S = N_S/\tau_R$, (b) averaged over the time interval $\tau_R = 2$ ms as well as over several realizations, are presented as functions of the eigenenergy of the proton-binding states on the rotor, E_0, at three values of the temperature, $T = 4.2$ K (liquid ^{4}He); $T = 77.2$ K (liquid ^{14}N); and $T = 300$ K. The other parameters, namely, the proton voltage, $V = 250$ mV, the normalized stator charge, $q = 1$, and the external torque, $\mathcal{T}_{\rm ext} = -41$ pN nm, correspond to the loaded F_0 motor. At resonant values of E_0, $E_0 \sim -90$ meV, and at high enough temperatures, $T > 50$ K, the motor works in a torque-generating regime characterized by a positive (CW) direction of rotation, $\langle\Omega\rangle > 0$, and positive current, $I_S > 0$, when protons flow downhill, from the source to the drain reservoir. In this regime both mechanisms, the power stroke and the Brownian ratchet, contribute to the torque generation.

At low temperatures, e.g., when $T = 4.2$ K, the ratchet mechanism practically turns off, and the system is not able to produce enough torque to execute the full-circle rotation in the presence of the counteracting load torque $\mathcal{T}_{\rm ext}$. In this shuttling mode, one proton-binding site oscillates back and forth between the source and drain channels, translocating the protons ($I_S > 0$), but no unidirectional rotation is generated ($\langle\Omega\rangle = 0$).

When $E_0 < -160$ meV the system is out of the transport windows, and the proton-binding sites on the rotor are always populated. Then, the rotor follows the negative external torque and rotates in the CCW direction without transferring protons (i.e., $\langle\Omega\rangle < 0$, $I_S \simeq 0$).

C. Torque generation and proton pumping

In Fig. 4 we show the dependence of (a) the average speed of rotations, $\langle\Omega\rangle/2\pi$, and (b) the average particle current, I_S (average number of protons transferred from the source channel per 1 ms), on the voltage V for the whole range of the CCW-directed external torque $\mathcal{T}_{\rm ext}$, from zero to −120 pN nm, at $E_0 = -90$ meV, and $T = 300$ K. For values of the external torque between zero and −80 pN nm and at a sufficiently high voltage, $V > 220$ meV, the motor performs a CW rotation [Fig. 4(a)] with a maximum frequency ~10 kHz (the torque-generating mode). In the process, protons flow downhill, from the source ($\mu_S = V/2$) to the drain channel ($\mu_D = -V/2$). The CCW-directed external torque hampers this motion, and when $|\mathcal{T}_{\rm ext}| > 80$ pN nm the rotation stops [Fig. 4(a)].

In the regime of ATP hydrolysis [13], the F_1 motor produces a sufficient torque to drive the rotation of the F_0 motor in the reverse (CCW) direction. In our case this regime takes place when $|\mathcal{T}_{\rm ext}| > 50$ pN nm, provided that the transmembrane potential is small enough, $V < 170$ meV [Fig. 4(a)]. It is evident from Fig. 4(b) that in this range of parameters the system works as a proton pump ($I_S < 0$), which translocates protons against the gradient of the electrochemical potential with a pumping efficiency

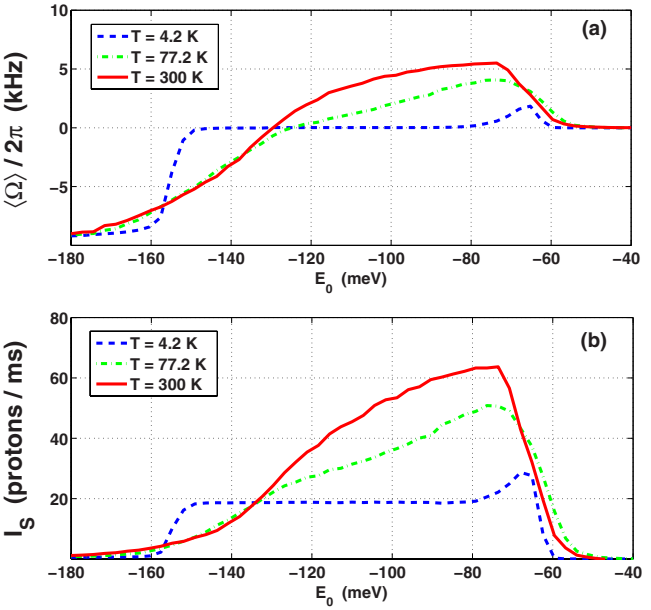

FIG. 3. (Color online) (a) The average frequency of rotations, $\langle\Omega\rangle/2\pi$ (in kHz), and (b) the average proton current I_S (the number of protons, transferred through the system in 1 ms) as functions of the energy of the rotor sites, E_0 (in meV), at $V = 250$ meV, $\mathcal{T}_{\rm ext} = -41$ pN nm, and at different temperatures, $T = 4.2$ K, $T = 77.2$ K, and $T = 300$ K. In the torque-generating regime ($T = 300$ K, $E_0 \sim -80$ meV), despite the counteracting load torque $\mathcal{T}_{\rm ext}$, the system rotates CW, $\langle\Omega\rangle > 0$, performing about five full circles [(a) red continuous line] and carrying more than 60 protons from the source to the drain in 1 ms (b). However, at very low temperatures, $T = 4.2$ K, the Brownian ratchet component of the torque-generating process turns off, and the rotor is not able to overcome the external torque. The system is now in the shuttling regime oscillating near a fixed position with zero average frequency of rotations, $\langle\Omega\rangle = 0$, but carrying about 20 protons per millisecond [(a) and (b) flat plateaus in the blue dashed curves].

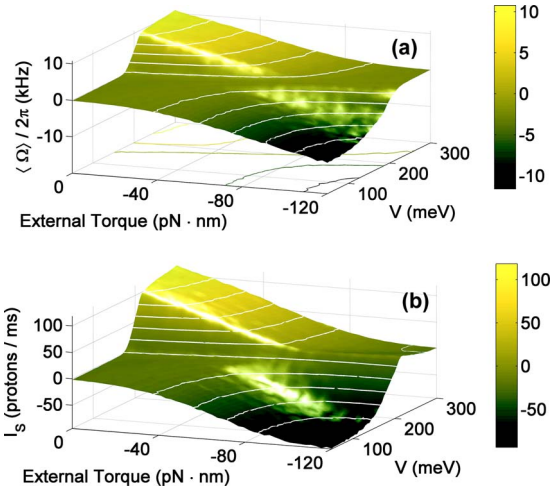

FIG. 4. (Color online) (a) The average speed of rotations $\langle\Omega\rangle/2\pi$ (in kHz), and (b) the average proton current, I_S, as functions of the proton voltage, V (in meV), and the external torque, $\mathcal{T}_{\text{ext}}$ (in pN nm), at $E_0=-90$ meV, and $T=300$ K. (a) shows that for a low enough counteracting load torque, $|\mathcal{T}_{\text{ext}}|<80$ pN nm, and at a high proton voltage, $V>220$ meV, the motor rotates clockwise with a maximum frequency of about 10 kHz. This rotation is accompanied by the positive proton current reaching the value $I_S \sim 100$ protons/ms (b). The dark (negative) regions in the figure correspond to the regime of ATP hydrolysis (pumping mode), when at low voltages, $V<170$ meV, the external torque, $|\mathcal{T}_{\text{ext}}|>50$ pN nm, is powerful enough to drive the motor rotation in the CCW direction ($\langle\Omega\rangle<0$), pumping protons ($I_S<0$) from the drain to the source against the proton electrochemical gradient V (b).

$$\mathcal{E}_{\text{pump}} = \frac{I_S V}{\mathcal{T}_{\text{ext}}\langle\Omega\rangle} \sim 20\% \tag{20}$$

when $V=100$ meV and $\mathcal{T}_{\text{ext}}=-108$ pN nm.

Note, that the voltage threshold for the torque-generating regime ($V>210$ meV when $\mathcal{T}_{\text{ext}}=-41$ pN nm) corresponding to the value of the electrochemical potential difference across the bacterial membrane and the inner mitochondrial membrane, is not preassigned *a priori*, but it is naturally determined by the configuration parameters of the model; for example, by the charge and the position of the stator as well as by the value of the load torque necessary to drive the ATP synthesis.

D. Contributions from the Brownian ratchet and power stroke components

The model studied here can be considered as a combination of Brownian ratchet and power stroke components [10,21]. The Brownian ratchet harnesses the energy of thermal fluctuations, biased by chemical reactions, to generate a unidirectional rotation. In our case, the ratchet component is introduced via a fluctuation force ξ, working in combination with the processes of loading and unloading protons in the presence of the confining potential U_{con} [see Eqs. (12) and (17)]. It is expected that the ratchet contribution should be significantly diminished at low temperatures.

The power stroke component is due to the Coulomb attraction between the positive stator charge, $q|e|$, and the negatively charged unoccupied rotor site. This part of the torque-generating process is proportional to the coefficient q, which is the stator charge, measured in units of $|e|$. For the torque-generating and pumping process in the F_0 motor of *E. coli*, the importance of the residue *c*Arg-210, carrying a positive charge, has been emphasized in Refs. [8,22].

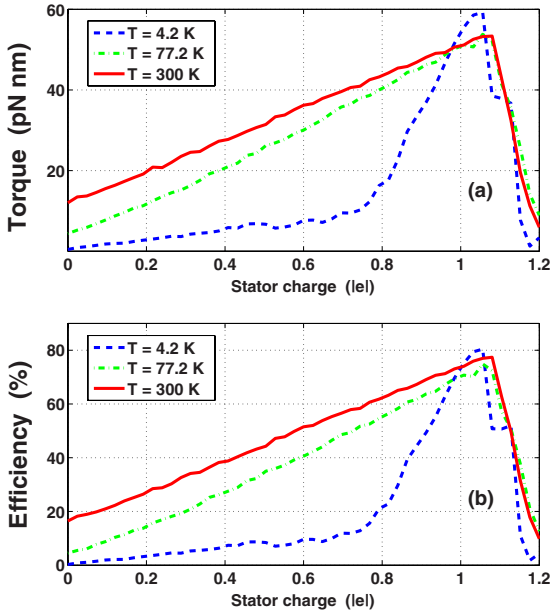

FIG. 5. (Color online) (a) Average torque, $\langle\mathcal{T}\rangle$ (in pN nm), and efficiency, $\mathcal{E}$, of the isolated motor ($\mathcal{T}_{\text{ext}}=0$) as functions of the normalized stator charge q (in units of $|e|$) for $V=250$ meV, $E_0=-90$ meV, and for three different temperatures: $T=4.2$ K (blue dashed line); $T=77.2$ K (green dashed-dotted line); and $T=300$ K (red continuous line). Without the stator charge [(a), red continuous line, $T=300$ K, $q\sim0$] the ratchet mechanism produces the torque ~12 pN nm, which is not enough to drive ATP synthesis. Near the optimal value of the stator charge ($q\sim1$), but at very low temperatures, $T=4.2$ K, the isolated motor generates the torque 60 pN nm by means of the power stroke mechanism [(a) blue dashed line]. This torque is higher than the CCW torque (−41 pN nm) necessary for ATP production. However, at these conditions, the F_0 motor coupled to the load ($\mathcal{T}_{\text{ext}}=-41$ pN nm) switches from the torque-generating mode to the shuttling regime, as shown in Fig. 3, and no average torque is produced. (b) demonstrates that the efficiency of the motor can reach $\simeq80\%$, when both components contribute to the torque-generating process.

In Fig. 5, taking the values $d=0.9$ nm, $E_0=-90$ meV, and V=250 meV, we plot (a) the average torque $\langle\mathcal{T}\rangle$ generated by the isolated motor (at $|\mathcal{T}_{\text{ext}}|=0$), and (b) the efficiency [14],

$$\mathcal{E} = \frac{\langle\mathcal{T}\rangle\langle\Omega\rangle}{I_S V}, \tag{21}$$

of the system as a function of the stator charge q, normalized by $|e|$, at low ($T=4.2$ K, dashed blue line), intermediate ($T=77.2$ K, dashed-dotted green line), and high ($T=300$ K, continuous red line) temperatures.

In the pure Brownian ratchet regime (no stator charge, $q=0$) the system generates a pronounced torque, $\langle\mathcal{T}\rangle$

~ 12 pN nm, if the temperature is high, $T=300$ K. However, this torque is not enough to overcome the load torque, $\mathcal{T}_{\text{ext}}=-41$ pN nm, which is necessary for ATP synthesis. For instance, at liquid Helium temperatures ($T=4.2$ K) the Brownian ratchet component is strongly suppressed.

Nevertheless, the power stroke mechanism can generate the torque $\langle \mathcal{T} \rangle_{\max} \simeq 60$ pN nm, which is higher than the load torque from the F_1 motor. The isolated F_0 motor demonstrates this peak value of the torque and the efficiency, $\mathcal{E}_{\max} \simeq 80\%$, at the stator charge near $|e|$ ($q \simeq 1$).

It follows from Fig. 3 that the power stroke component alone is not able to drive ATP synthesis, because at the load conditions, $\mathcal{T}_{\text{ext}}=-41$ pN nm, and at $T=4.2$ K, the system operates in the shuttling mode, with a proton current but generating no unidirectional motion. Notice also that despite the presence of a medium with high viscosity coefficient, $\eta=1$ Pa s$=1000\,\eta_{\text{water}}$, and despite the very small size, $r_0=3$ nm, the motor performs quite well and generates a significant torque at physiologically reasonable parameters.

Note that, because of the asymmetric configuration, this motor does not produce a unidirectional torque for a negative electrochemical potential difference ($V<0$), but it switches the direction of rotation if the drain channel (see Fig. 1) is placed on the other side of the source channel (at $\phi_D=\pi+\phi_0$). This feature, as well as the nanoelectromechanical method as a whole, can be useful for explaining the switching ability of bacterial flagellar motors, which allows the chemotaxis of bacteria [14,16].

V. CONCLUSIONS

We have examined a simple nanoelectromechanical model of a proton-driven rotary nanomotor which mimics the basic operating principles and the configuration of the F_0 motor of ATP synthase in bacterial and mitochondrial membranes. Treating ATP synthase as a nonequilibrium open system, coupled to two proton reservoirs, we have derived a set of rate equations, which describes the loading and unloading of the proton-binding sites on the rotor portion of the motor.

At normal conditions, the isolated motor generates a torque of about 60 pN nm with efficiency near 80%, whereas the motor working against a constant load, created by the F_1 portion, exhibits a unidirectional rotation (Fig. 2) with frequency ~ 4 kHz. It is shown that, depending on the temperature T, the external torque $\mathcal{T}_{\text{ext}}$, the proton voltage build-up V, and the energy E_0 of the rotor sites, the system operates in three different regimes: The torque-generating mode; the shuttling regime; and the pumping mode (see Fig. 3 and Fig. 4).

In the torque-generating mode, energy (stored in the gradient of the proton electrochemical potential) is converted into mechanical energy of the rotor. This energy transfer drives the unidirectional rotation of the motor, $\langle \Omega \rangle > 0$, and the positive particle current, $I_S > 0$, corresponding to the downhill flow of protons from the periplasmic (P) to the cytoplasmic (N) side of the membrane.

In the shuttling regime, which takes place at low temperatures, the rotor vibrates with a small amplitude near the initial point without performing a full circle. In doing so, the proton-binding site, located between the source and drain half-channels, works as a nanomechanical shuttle carrying protons from the P side to the N side of the membrane. This regime is distinguished by zero-frequency rotations, $\langle \Omega \rangle = 0$, and by a positive proton current, $I_S > 0$.

In the pumping mode [8,13], ATP synthase operates in reverse, where ATP hydrolysis drives rotations of the F_1 motor. This external torque, $\mathcal{T}_{\text{ext}}$, is transmitted to the F_0 motor, which pumps protons uphill, from the N to P membrane side. In our case, the CCW-directed external torque, $\mathcal{T}_{\text{ext}}=-120$ pN nm, is enough to translocate, in 1 ms, about 90 protons against the electrochemical gradient of 100 meV [see Fig. 4(b)].

We have studied the performance of the model at different temperatures and found that this performance depends significantly on the Coulomb interaction, U_q, between the positive stator charge and the negatively charged empty rotor site. The torque produced by the Brownian ratchet mechanism alone is not sufficient to overcome the load torque from the F_1 motor. A key feature of the model is that, because of Coulomb coupling to the stator charge, the energy of the proton on the rotor site, which is close to the source half-channel, $E(\phi_S)$, is higher, than the proton energy of the site located near the outlet of the drain channel, $E(\phi_D)$.

For positive proton voltage V, when the electrochemical potential of the source, $\mu_S = V/2$, exceeds the potential of the drain, $\mu_D = -V/2$, the rotor sites can be loaded with protons at the source and unloaded at the drain, if the energies $E(\phi_S)$ and $E(\phi_D)$ fit the transport window: $\mu_S > E(\phi_S) > E(\phi_D) > \mu_D$. This energy difference, $\Delta E = E(\phi_S) - E(\phi_S) = U_q(\phi_D) - U_q(\phi_S)$, is directly converted into mechanical energy. It is shown, however, that at low temperatures, when the Brownian ratchet component is suppressed, the motor works in the shuttling mode, and no torque is generated. This means that, in agreement with previous results [8,11], the power stroke and the Brownian ratchet components should work together for the efficient operation of the system. These conclusions can be applied both to biological rotary motors and to artificial nanoengines. Notice also that an efficient and powerful future synthetic motor based on this bioinspired design would be expected to withstand a more severe environment, in particular, much lower temperatures, than its biological counterparts. The present design can be compared with modern industrial electrical motors having an efficiency about 90%. However, it should be emphasized that this efficiency decreases drastically when decreasing the size of the motors. Nanoscale motors operating in a warm and very viscous medium, even with an efficiency 80%, are worth building and studying as a function of various operating conditions.

ACKNOWLEDGMENTS

This work was supported in part by the National Security Agency, Laboratory of Physical Science, Army Research Office, National Science Foundation Grant No. EIA-0130383, Contract No. JSPS-RFBR 06-02-91200, and Core-to-Core (CTC) program supported by the Japan Society for Promotion of Science (JSPS). S.S. acknowledges support from the EPSRC ARF Contract No. EP/D072581/1 and AQDJJ network programme. L.M. was partially supported by the NSF NIRT, Grant No. ECS-0609146.

[1] B. Alberts, A. Johnson, J. Lewis, M. Raff, K. Roberts, and P. Walter, *Molecular Biology of the Cell* (Garland Science, New York, 2002), Chaps. 11 and 14.
[2] W. R. Browne and B. L. Feringa, Nat. Nanotechnol. **1**, 25 (2006).
[3] M. Wikström, Biochim. Biophys. Acta **1655**, 241 (2004); G. Bränden, R. B. Gennis, and P. Brzezinski, *ibid.* **1757**, 1052 (2006).
[4] Y. C. Kim, M. Wikström, and G. Hummer, Proc. Natl. Acad. Sci. U.S.A. **104**, 2169 (2007).
[5] A. Yu. Smirnov, L. G. Mourokh, and F. Nori, Phys. Rev. E **77**, 011919 (2008).
[6] A. N. Glagolev and V. P. Skulachev, Nature (London) **272**, 280 (1978).
[7] W. Junge, H. Lill, and S. Engelbrecht, Trends Biochem. Sci. **22**, 420 (1997); W. Junge, Proc. Natl. Acad. Sci. U.S.A. **96**, 4735 (1999).
[8] T. Elston, H. Wang, and G. Oster, Nature (London) **391**, 510 (1998).
[9] P. Dimroth, H. Wang, M. Grabe, and G. Oster, Proc. Natl. Acad. Sci. U.S.A. **96**, 4924 (1999).
[10] G. Oster and H. Wang, Trends Cell Biol. **13**, 114 (2003).
[11] A. Aksimentiev, I. A. Balabin, R. H. Fillingame, and K. Schulten, Biophys. J. **86**, 1332 (2004).
[12] R. A. Capaldi and R. Aggeler, Trends Biochem. Sci. **27**, 154 (2002).
[13] P. Dimroth, C. von Ballmoos, and T. Meier, EMBO Rep. **7**, 276 (2006); C. von Ballmoos, G. M. Cook, and P. Dimroth, Annu. Rev. Biophys. **37**, 43 (2008).
[14] H. C. Berg, Annu. Rev. Biochem. **72**, 19 (2003).
[15] J. Xing, F. Bai, R. Berry, and G. Oster, Proc. Natl. Acad. Sci. U.S.A. **103**, 1260 (2006).
[16] M. Inoue and K. Kaneko, Phys. Rev. E **74**, 011903 (2006); Q. Wen *et al.*, J. Stat. Phys. **128**, 257 (2007).
[17] A. Y. Mulkidjanian, Biochim. Biophys. Acta **1757**, 415 (2006).
[18] P. Reimann, Phys. Rep. **361**, 57 (2002).
[19] P. Hänggi, F. Marchesoni, and F. Nori, Ann. Phys. **14**, 51 (2005).
[20] S. Savel'ev and F. Nori, Chaos **15**, 026112 (2005); F. Nori, Nat. Phys. **2**, 227 (2006).
[21] H. Wang and G. Oster, Appl. Phys. A: Mater. Sci. Process. **75**, 315 (2002).
[22] B. D. Cain and R. D. Simoni, J. Biol. Chem. **264**, 3292 (1989).
[23] N. S. Wingreen, A.-P. Jauho, and Y. Meir, Phys. Rev. B **48**, 8487 (1993).
[24] J. R. Johansson, L. G. Mourokh, A. Yu. Smirnov, and F. Nori, Phys. Rev. B **77**, 035428 (2008).
[25] R. I. Shekhter, Yu. Galperin, L. Y. Gorelik, A. Isacsson, and M. Jonson, J. Phys.: Condens. Matter **15**, R441 (2003); M. Blencowe, Phys. Rep. **395**, 159 (2004).
[26] J. K. Gimzewski *et al.*, Science **281**, 531 (1998); A. M. Fennimore *et al.*, Nature (London) **424**, 408 (2003); G. S. Kottas *et al.*, Chem. Rev. (Washington, D.C.) **105**, 1281 (2005).
[27] F. Bartl, G. Deckers-Habestreit, K. Altendorf, and G. Zundel, Biophys. J. **68**, 104 (1995).
[28] O. Y. Dmitriev, P. C. Jones, and R. H. Fillingame, Proc. Natl. Acad. Sci. U.S.A. **96**, 7785 (1999).
[29] V. K. Rastorgi and M. E. Girvin, Nature (London) **402**, 263 (1999).
[30] J. Howard, *Mechanics of Motor Proteins and the Cytoskeleton* (Sinauer Associates, Sunderland, MA, 2001).
[31] Y. R. Nartsissov and E. V. Mashkovtseva, J. Theor. Biol. **242**, 300 (2006).